Structural modification of the cation-ordered Ruddlesden-Popper phase $YSr_2Mn_2O_7$ by cation exchange and anion insertion.

Ronghuan Zhang[†], Alexandra S. Gibbs[‡], Weiguo Zhang[§], P. Shiv Halasyamani[§] and Michael A. Hayward [†]*

[†] Department of Chemistry, University of Oxford, Inorganic Chemistry Laboratory, South Parks Road, Oxford, OX1 3QR, U. K.

[‡] ISIS Facility, Rutherford Appleton Laboratory, Chilton, Oxon OX11 0QX, U. K.

[§] Department of Chemistry, University of Houston, 112 Fleming Building, Houston, Texas 77204-5003, U. S. A.

Supporting Information Placeholder

ABSTRACT: Calcium-for-strontium cation substitution of the $a^-b^0c^0/b^0a^-c^0$ distorted, cation ordered, n = 2 Ruddlesden-Popper phase, $YSr_2Mn_2O_7$, leads to separation into two phases which both retain an $a^-b^0c^0/b^0a^-c^0$ distorted framework and have the same stoichiometry, but exhibit different degrees of Y/Sr/Ca cation order. Increasing the calcium concentration to form $YSr_{0.5}Ca_{1.5}Mn_2O_7$ leads to a change in the cooperative tilting on the MnO_6 units to a novel $a^-b^-c^-/b^-a^-c^-$ arrangement described in space group $P2_1/n11$. Low-temperature, topochemical fluorination of $YSr_2Mn_2O_7$ yields $YSr_2Mn_2O_{5.5}F_{3.5}$. In contrast to many other fluorinated n = 2 Ruddlesden-Popper oxide phases, $YSr_2Mn_2O_{5.5}F_{3.5}$ retains the $a^-b^0c^0/b^0a^-c^0$ lattice distortion and $P4_2/mnm$ space group symmetry of the parent oxide phase. The resilience of the $a^-b^0c^0/b^0a^-c^0$ distorted framework of $YSr_2Mn_2O_7$ to resist symmetry changing deformations on both cation substitution and anion insertion/exchange is discussed on the basis the A-site cation order of the lattice and the large change in the ionic radius of manganese on oxidation from $Mn^{3+}$to Mn^{4+}. The structure property relations observed in the Y-Sr-Ca-Mn-O-F system provide insight to assist in the synthesis of n = 2 Ruddlesden-Popper phases which adopt cooperative structural distortions which break the inversion symmetry of the extended lattice, and therefore act as a route for the preparation of ferroelectric and multiferroic materials.

Introduction

The chemical diversity of oxide phases which adopt ABO_3 perovskite structures can be attributed in part to the high mechanical flexibility of the perovskite framework. This flexibility allows the apex-linked BO_6 octahedra, which constitute the perovskite framework, to cooperatively tilt and twist to optimize the packing of the system in response to changes in the ratio of the A- and B-cation radii (conveniently parameterized by the structural tolerance factor: $t = \langle A\text{-}O\rangle/\sqrt{2}\langle B\text{-}O\rangle$).[1] As a result a wide range of cation combinations can be incorporated into thermodynamically stable perovskite lattices.

A further feature of the tilting and twisting distortions of perovskite phases is that they can be harnessed to modify and tune the physical behavior of systems, particularly transition-metal containing phases. This is because the collective rotations of the octahedra act to distort the B-O-B bond angles from the 180º value observed in the undistorted, aristotype framework. This tightening of the B-O-B bond angles modifies the orbital interactions and thus the coupling between the local electronic states of the transition metal B-cations, changing electronic band widths in electronically delocalized systems, or magnetic exchange interactions in localized systems.[2] As a result much effort has gone into understanding the electronic and magnetic consequences of tuning the structural distortions of perovskite phases, typically via studies which make chemical substitutions on the 12-coordinate A-site.[2-3]

In addition to tuning the electronic coupling between neighboring B-cations, the collective distortions of perovskite phases also modify the lattice symmetry of the framework. As a consequence, if the correct distortion mode is adopted, the collective deformations of perovskite lattices offer a mechanism to break the inversion symmetry of the system, and thus the potential to induce ferroelectric behavior.[4] In the specific case of the three-dimensional perovskite lattice, acentric phases can only be produced when octahedral tilting is accompanied by cation order.[5-8] However, when the equivalent structural distortions are applied to layered analogues of the perovskite structure, particularly $A_3B_2O_7$, n = 2 Ruddlesden-Popper phases, the inversion symmetry of the system can be broken in the absence of cation order,[9-10] as demonstrated by the observation of ferroelectric behavior in $(Ca, Sr)_3Ti_2O_7$.[11]

Utilizing the distortions of n = 2 Ruddlesden-Popper phases to prepare non-centrosymmetric lattices is highly attractive because it provides a route to polar materials without the need to include 'active distortion centers', such as d^0 transition metal cations, which break inversion symmetry through the action of a second-order Jahn Teller (SOJT) distortion.[12-15] The additional chemical flexibility which comes from not having to include such centers makes the incorporation of paramagnetic ions into polar frameworks much easier, and thus distorted n = 2 Ruddlesden-Popper

phases offer a route to the preparation of magnetoelectric multiferroic materials.

While the distortions of $n = 2$ Ruddlesden-Popper phases offer an attractive route for the preparation of non-centrosymmetric phases in theory, it is hard to realize these concepts in practice because the desired '$A2_1am$', $a^-a^-c^+$/ $a^-a^-c^+$ ferroelectric distortion mode is only stabilized at extremely low values of the structural tolerance factor. A recent study by Pitcher et al. highlighted these difficulties when they observed that it was not possible to induce the desired polar distortion mode in the Fe^{3+}, $Ln_2AEFe_2O_7$ (Ln = lanthanide; AE = Ba, Sr, Ca) system through A-site substitution.[16] This was partly because in compositions containing very small A-cations, $A_3B_2O_7$ $n = 2$ Ruddlesden-Popper phases tend to be thermodynamically less stable than a 1:1 mixture of the corresponding A_2BO_4 n = 1 Ruddlesden-Popper phase and the ABO_3 perovskite. Thus in the $Ln_2AEFe_2O_7$ system, the $A2_1am$ distorted structure could only be stabilized by additional titanium-for-iron B-site substitution.[16]

In an attempt to circumvent these problems, we have been looking at the use of topochemical manipulation as a route to prepare non-centrosymmetric materials. Specifically we have been utilizing the observation that fluorine insertion leads to a significant enhancement of the lattice distortions of many $n = 2$ Ruddlesden-Popper systems, as indicated by a general tightening of the B-O-B bond angles.[17-20] Furthermore it has also been observed that on fluorination the largest enhancement tends to be to the rotations of the BO_6 octahedra around the crystallographic *z*-axis. This led us to anticipate that the fluorination of $La_3Ni_2O_7$, which adopts an Amam, $a^-a^-c^0$/ $a^-a^-c^0$ distortion, would lead to the formation of an oxide-fluoride phase with the desired polar $A2_1am$, $a^-a^-c^+$/ $a^-a^-c^+$ distorted structure. However, detailed crystallographic study of $La_3Ni_2O_{5.5}F_{3.5}$ reveals that while fluorination of $La_3Ni_2O_7$ does induce a *z*-axis rotation of the NiX_6 octahedra, the 'sense' of this rotation (clockwise or anti-clockwise) alternates between adjacent perovskite sheets to yield an $a^-a^-c^+$/ a^-a^- -(c^+) distortion which breaks the inversion symmetry of the lattice locally, but not globally, yielding an antiferroelectric lattice with *Pnma* space group symmetry.[19] While this synthesis did not achieve the desired result, it shows that the basic concept is viable and motivates us to study the fluorination of other systems to see if it is possible to prepare a fluorinated phase which is ferroelectric rather than antiferroelectric

In this contribution we report the effects of A-cation substitution and topochemical fluorine insertion on the structure of A-cation ordered, $n = 2$ Ruddlesden-Popper phase $YSr_2Mn_2O_7$. It was hoped that these chemical modifications would enhance the collective distortions of the layered perovskite phase, leading to a non-centrosymmetric, polar material.

Experimental

Synthesis. Samples in the $YSr_{2-x}Ca_xMn_2O_7$ series (x = 0, 0.25, 0.5, 1.0 and 1.5) were prepared via a citrate gel method. Suitable stoichiometric ratios of Y_2O_3 (99.99%, dried at 900 °C), $SrCO_3$ (99.99%), $CaCO_3$ (99.99%) and MnO_2 (99.9%) were dissolved in a minimal quantity of 6 M nitric acid. Citric acid and ethylene glycol were then added, and the solution was heated with constant stirring. The gel thus formed was heated to 350 °C until a coarse black powder was obtained. The powder was ground and then heated to 1000 °C in air at a rate of 1 °C/min to remove the remaining organic components. The resulting powder was then pressed into pellets before further heat treatments. For the preparation of $YSr_2Mn_2O_7$ and $YSr_{1.75}Ca_{0.25}Mn_2O_7$, the sample pellets were heated for 3 periods of 48 h at 1350 °C in air and 2 further periods of 48 h at 1450 °C. For $YSrCaMn_2O_7$, the pellets were heated for 3 periods of 48 h at 1350 °C in air and 2 further periods of 48 h at 1400 °C. For $YSr_{0.5}Ca_{1.5}Mn_2O_7$, the pellets were heated for 5 periods of 48 h at 1350 °C in air. Lower synthesis temperatures were employed for the calcium substituted samples to avoid melting. The preparation of $YCa_2Mn_2O_7$ was also attempted, but the phase failed to form after 4 heating cycles of 48 hours at 1300 °C and this composition melts at 1325 °C.

Fluorination of $YSr_2Mn_2O_7$ and $YSr_{0.5}Ca_{1.5}Mn_2O_7$ was carried out using CuF_2 as a fluorination agent, in the same manner as has been described previously.[17, 20-21] To avoid contamination of the samples with CuO which occurs when the fluorination agent is mixed directly into the sample, the CuF_2 was heated separately from the sample at 500 °C under flowing oxygen to liberate fluorine. The resulting O_2/F_2 gas mixture was then passed over a sample of $YSr_{2-x}Ca_xMn_2O_7$ powder, held at 400 °C in adjacent furnace. Samples were treated in this way for 4 periods of 48 h, with the CuF_2 reagent being replaced between heating periods.

Characterization. X-ray powder diffraction data were collected using a PANalytical X'pert diffractometer incorporating an X'celerator position sensitive detector (monochromatic Cu $K_{\alpha 1}$ radiation). Neutron powder diffraction data were collected from samples contained within vanadium cans, using the HRPD diffractometer (ISIS neutron source, U.K). Rietveld profile refinement was performed using the GSAS suite of programs.[22] Magnetization data were collected using a Quantum Design MPMS SQUID magnetometer. Average manganese oxidation states were determined by iodometric titration. Titrations were performed by dissolving samples in a dilute HCl solution containing an excess of KI and titrating the amount of liberated I_2 with standardized $Na_2S_2O_3$ solution. Powder second-harmonic generation (SHG) measurements were performed on a modified Kurtz-Perry instrument.[23] A description of the equipment and methodology has been published previously.[24]

Results

Structural characterization of $YSr_2Mn_2O_7$ ($0 < x < 1.5$). X-ray powder diffraction data collected from samples of $YSr_{2-x}Ca_xMn_2O_7$ (x = 0, 0.25, 0.5, 1, 1.5), shown in Figure 1,

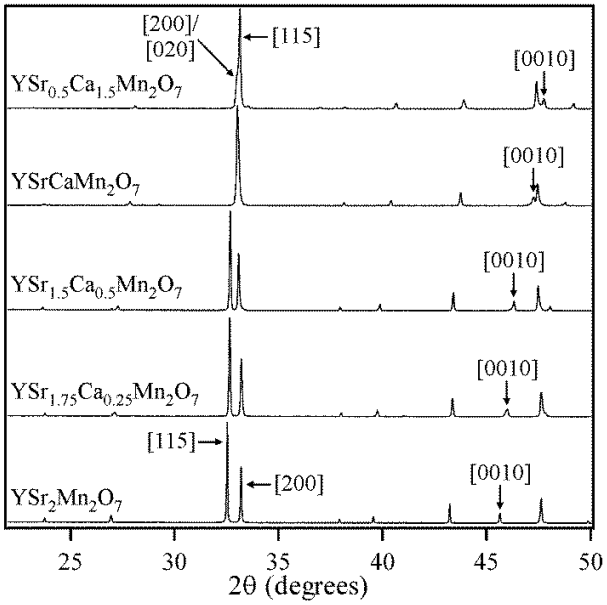

Figure 1. X-ray powder diffraction data collected from $YSr_{2-x}Ca_xMn_2O_7$.

were initially indexed on the basis of tetragonal unit cells, consistent with the formation of n = 2 Ruddlesden-Popper phases. Structural models based on the $a^-b^0c^0$/ $b^0a^-c^0$ distorted n = 2 Ruddlesden-Popper structure of $YSr_2Mn_2O_7$ (space group $P4_2/mnm$),[25] but with calcium partially replacing strontium as appropriate, were refined against these data. The refinements proceeded smoothly, however close inspection revealed that, with the exception of the x = 0 sample, none of the fits to the data were satisfactory.

Detailed inspection of the data from the x = 0.25, 0.5, 1 samples revealed that the poor fitting of the $P4_2/mnm$ structural model was due to a peak shape asymmetry of the 00l diffraction reflections. This asymmetry could not be modelled by the addition of *hkl* dependent broadening terms, however the fits to the data were significantly improved by the introduction of a second tetragonal n = 2 Ruddlesden-Popper phase to the models.

In order to stabilize these 2-phase refinements the peak shapes and atomic positions of the two phases were constrained to be the same, with only the lattice parameters and phase fractions of the two phases allowed to refine freely. Table 1 shows the refined values of these parameters.

x		a (Å)	c (Å)	Volume (Å^3)	Fraction
0		5.40456(6)	19.9054(2)	581.26(2)	100%
0.25	P1	5.4064(1)	19.7608(3)	577.26(1)	66.5(6)%
	P2	5.3997(1)	19.7883(5)	576.98(2)	33.5(6)%
0.5	P1	5.4106(1)	19.5848(1)	573.33(1)	83.7(2)%
	P2	5.4006(1)	19.6388(5)	572.81(2)	16.3(2)%
1	P1	5.4254(1)	19.255(1)	566.79(1)	65.8(1)%
	P2	5.4123(1)	19.325(1)	566.11(3)	34.2(1)%

Table 1. The lattice parameters from 2-phase refinements of $YSr_{2-x}Ca_xMn_2O_7$. Parameters from the x = 0 composition extracted from ref [25].

Structural characterization of $YSrCaMn_2O_7$. Phase separation analogous to that observed for $YSr_{2-x}Ca_xMn_2O_7$ (0.25 < x < 1) has been observed in other manganese-containing n = 2 Ruddlesden-Popper phases.[26-28] To further investigate the phase separation of the $YSr_{2-x}Ca_xMn_2O_7$ system, high resolution neutron powder diffraction data were collected from $YSrCaMn_2O_7$.

In common with the X-ray data, satisfactory fits to the neutron powder diffraction data collected from $YSrCaMn_2O_7$ could only be achieved using 2-phase models, however the high resolution of the latter data set allowed the atomic coordinates and site occupancies of the two phases to be refined independently. To assist refinement stability the thermal displacement factors of corresponding atoms in the two phases were constrained to be the same.

The origin of the observed phase separations in manganese-containing n = 2 Ruddlesden-Popper phases has been variously ascribed to either A-cation inhomogeneity within samples (i.e. the 2 phases have different chemical compositions) or to a difference in A-cation distribution on the 9-fold and 12-fold A-cation coordination sites in the different phases (i.e. the 2 phases have the same composition but different A-cation orderings).[26] In order to determine which of these scenarios is responsible for the phase separation in the $YSr_{2-x}Ca_xMn_2O_7$ system, the structural refinement of $YSrCaMn_2O_7$ was initially performed with the constraint that the two tetragonal phases in the structural model had the same, ideal, chemical composition: $YSrCaMn_2O_7$ (neutron scattering lengths: Ca 4.70 fm; Y 7.75 fm; Sr 7.02 fm).[29] The refinement proceed smoothly with this constraint to give a good statistical fit (χ^2 = 5.79) producing a structural model in which the Y:Sr:Ca distributions over the 9-fold (Phase 1 = 50:4:46; Phase 2 = 50:10:40) and 12-fold (Phase 1 = 0:91:9; Phase 2 = 0:80:20) A-cation sites differed between the two phases. The A-cation distribution constraint was then released so that the occupancies of the A-cation sites in the 2 phases could vary freely and thus the chemical compositions of the two phases could vary freely. With the removal of this constraint it was observed that none of the A-site neutron scattering powers changed by more than 1%, indicating that the principal difference between the 2 phases of $YSrCaMn_2O_7$ is their A-cation ordering, not their chemical composition. A full description of the refined 2-phase structural model of $YSrCaMn_2O_7$ is given in Table S1, with selected bond lengths and angles in Table S2 and plots of the observed and calculated data shown in Figure S1 in the Supporting Information.

Structural characterization of $YSr_{0.5}Ca_{1.5}Mn_2O_7$. Detailed inspection of X-ray powder diffraction data collected from $YSr_{0.5}Ca_{1.5}Mn_2O_7$ revealed that the poor fitting of the $P4_2/mnm$ structural model was due to a splitting of diffraction peaks, consistent with a lowering of the crystallographic symmetry from tetragonal to orthorhombic. As noted above, calcium substitution into the $YSr_{2-x}Ca_xMn_2O_7$ will reduce the structural tolerance factor of the system leading to an enhancement of the collective tilting and twisting distortions of the MnO_6 octahedra. The lower crystallographic symmetry of the x = 1.5 sample therefore suggests it has a more distorted structure than the x < 1.5 samples. Starting from the $a^-b^0c^0$/ $b^0a^-c^0$ distortion of the 0 < x < 1 phases, the symmetry analysis performed by Aleksandrov and Bartolome [30] indicates there are 6 possible collective distortions that $YSr_{0.5}Ca_{1.5}Mn_2O_7$ could adopt, as detailed in Table 2. Structural models were constructed for each of these 6 distorted n = 2 Ruddlesden-Popper frameworks and then refined against neutron powder diffraction data collected from $YSr_{0.5}Ca_{1.5}Mn_2O_7$. It was assumed that the 12-coordinate A-sites contained a 1:1 mixture of Sr:Ca, and the 9-coordinate A-sites contained a 1:1 mixture of Y:Ca. Subsequent refinement of these parameters showed this to be the case, so all models were fixed with these A-site compositions. In addition, displacement parameters were constrained by element. All 6 refinements converged smoothly.

The goodness of fit parameters listed in Table 2 indicate that the 3 A-centered models describing $a^-a^-c^?/a^-a^-c^?$ distortions give much poorer fits to the data than the 3 primitive models which describe $a^-b^-c^?/b^-a^-c^?$ distortions, eliminating the former models from consideration. Of the three remaining models the $a^-b^-c^-/b^-a^-c^-$ distorted $P2_1/n11$ model has the best fitting statistics, considerably better than the $a^-b^-c^0/b^-a^-c^0$ distorted $Pnnm$ model, but only marginally better than the $a^-b^-c^+/b^-a^-c^+$ distorted $P2_1nm$ model. In order to help to differentiate between the $P2_1nm$ and $P2_1/n11$ models we investigated the SHG activity of $YSr_{0.5}Ca_{1.5}Mn_2O_7$ as an $a^-b^-c^+/b^-a^-c^+$ distorted $P2_1nm$ structure would be non-centrosymmetric, and thus SHG active, while a $a^-b^-c^-/b^-a^-c^-$ distorted $P2_1/n11$ structure would be centrosymmetric and thus SHG inactive. No SHG activity was observed for $YSr_{0.5}Ca_{1.5}Mn_2O_7$, consistent with this phase adopting an $a^-b^-c^-/b^-a^-c^-$ distorted $P2_1/n11$ structure. Full details for the refined structure of $YSr_{0.5}Ca_{1.5}Mn_2O_7$ are given in Table S3, with selected bond lengths and angles in Table S2 and a plot of the observed and calculated data is shown in Figure S2, in the Supporting Information.

Space group	distortion	χ^2	wRp(%)	Rp(%)
$P2_1/n11$ (#14)	$a^-b^-c^-/b^-a^-c^-$	7.63	4.74	4.95
$P2_1nm$ (#31)	$a^-b^-c^+/b^-a^-c^+$	7.71	4.77	5.01
$Pnnm$ (#58)	$a^-b^-c^0/b^-a^-c^0$	8.19	4.92	5.08
$A2_1am$ (#36)	$a^-a^-c^+/a^-a^-c^+$	17.09	7.14	6.30
$A2/a$ (#15)	$a^-a^-c^-/a^-a^-c^-$	17.79	7.28	6.42
$Amam$ (#63)	$a^-a^-c^0/a^-a^-c^0$	17.11	7.15	6.31

Table 2. Fitting statistics from the structural refinement of $YSr_{0.5}Ca_{1.5}Mn_2O_7$ using models based on the distortions of n = 2 Ruddlesden-Popper phases.

Fluorination of $YSr_{2-x}Ca_xMn_2O_7$. The fluorination of $YSr_2Mn_2O_7$, by the procedure outlined above, yielded a single phase sample with an expanded *c*-lattice parameter, consistent with topochemical fluorination to form a phase of composition $YSr_2Mn_2O_xF_y$. In contrast, when the same procedure was applied to $YSr_{0.5}Ca_{1.5}Mn_2O_7$, a mixture of apparently unreacted material and a new tetragonal phase, nominally assigned as $YSr_{0.5}Ca_{1.5}Mn_2O_xF_y$, was observed with an approximate stoichiometric ratio of 3:1. Further fluorination cycles led to no further reaction, and raising the reaction temperature led to decomposition and the formation of binary fluorides (SrF_2, CaF_2, etc.), indicating the calcium-doped phase could not be readily fluorinated via this route.

Chemical and structural characterization of $YSr_2Mn_2O_{5.5}F_{3.5}$. The crystallographic characterization of $YSr_2Mn_2O_xF_y$, described below, indicates that this is a fluorine intercalated n = 2 Ruddlesden-Popper phase in which all the anion sites were fully occupied and thus x + y = 9, as observed for other fluorinated n = 2 Ruddlesden-Popper phases.[17-20, 31] This information, combined with iodometric titration results which revealed an average manganese oxidation state of Mn +3.75, indicate the fluorinated phase has a chemical formula of $YSr_2Mn_2O_{5.5}F_{3.5}$.

Neutron powder diffraction data collected from $YSr_2Mn_2O_{5.5}F_{3.5}$ can be readily indexed using a tetragonal unit cell (a = 5.326 Å, c = 22.631 Å) with extinction conditions consistent with the $P4_2/mnm$ space group symmetry of the all-oxide starting material $YSr_2Mn_2O_7$. A structural model was constructed in space group $P4_2/mnm$, based on the reported structure of $YSr_2Mn_2O_7$ but with additional anions inserted into the 'tetrahedral' coordination sites within the rock salt layers of the phase, in an analogy to the structures of a series of other fluorine intercalated n = 2 Ruddlesden-Popper oxide phases.[17, 19-20] The Y/Sr distribution was set to be the cation-ordered arrangement observed for the $YSr_2Mn_2O_7$ parent phase. Refinement of this model against the neutron powder diffraction data proceeded smoothly. All atomic positional and displacement parameters were refined freely. Given the very similar neutron scattering lengths of oxide and fluoride (O = 5.80 fm; F = 5.65 fm)[29] no attempt was made to differentiate between the two anions at this stage, with all anion sites treated as if they were occupied by oxide. The refinement converged smoothly to give a good statistical fit (χ^2 = 5.43).

The majority of previous studies which have examined analogous fluorinations of n = 2 Ruddlesden-Popper oxides, observe a lowering of crystallographic symmetry on fluorine insertion.[17-19] Therefore to confirm that the model in space group $P4_2/mnm$ is the best description of the structure of $YSr_2Mn_2O_{5.5}F_{3.5}$, a series of lower symmetry models, with more distorted $Mn(O/F)_6$ networks, and also with disordered $Mn(O/F)_6$ rotations, were refined against the neutron powder diffraction data. As shown in Table S5 in the Supporting Information, none of these models achieve as good a statistical fit as the $P4_2/mnm$ model, confirming this is the best structural description of $YSr_2Mn_2O_{5.5}F_{3.5}$.

As noted above, the poor neutron scattering contrast between oxide and fluoride ions prevents the anion distribution in $YSr_2Mn_2O_{5.5}F_{3.5}$ being determined directly. However it is possible in some cases to deduce the location of fluoride ions within oxide-fluoride lattices by examining the local bonding environments of anion sites through bond valence sums (BVS).[32-34] This approach has proved effective in locating the fluoride ions in a number of fluorinated n = 2 Ruddlesden-Popper phases.[18-20]

Table 3 lists the BVS of the 7 crystallographically distinct anion sites in the structure of $YSr_2Mn_2O_{5.5}F_{3.5}$. These BVS values were calculated the basis of occupation by oxide or fluoride, and the BVS values of corresponding anion sites in the structure of $YSr_2Mn_2O_7$ were also calculated for comparison. The anion site labelling scheme is shown in Figure 2. These data reveal that the two smallest BVS values were calculated from the tetrahedral interstitial anion sites X(6) and X(7), consistent with the occupation of fluoride ions. Occupation of the 'interstitial' anion sites exclusively by fluoride ions has been observed widely in other topochemically fluorinated n = 2 Ruddlesden-Popper oxide phases.[17-20] The composition of the fluorinated phase requires fluoride ions to have been exchanged with oxide ions of the 'parent' oxide phase.

The data in Table 3 show that the BVS of the 'apical' X(1) site is the lowest of the remaining anion sites, suggesting that it is occupied by a 3:1 mixture of $F^-:O^{2-}$ to make up the overall $YSr_2Mn_2O_{5.5}F_{3.5}$ stoichiometry. Similarly preferential substitution of fluoride for oxide at the apical anion site has been observed in other topochemically fluorinated phases such as $Sr_3(Fe_{0.5}Ru_{0.5})_2O_{5.5}F_{3.5}$ and $La_3Ni_2O_{5.5}F_{3.5}$.[18-19] Full details for the refined structure of $YSr_2Mn_2O_{5.5}F_{3.5}$ are given in Table S6, with selected bond lengths and angles in Table S2 and a plot of the observed and calculated data is shown in Figure S3 in the Supporting Information. A representation of the structure of $YSr_2Mn_2O_{5.5}F_{3.5}$ is shown in Figure 2.

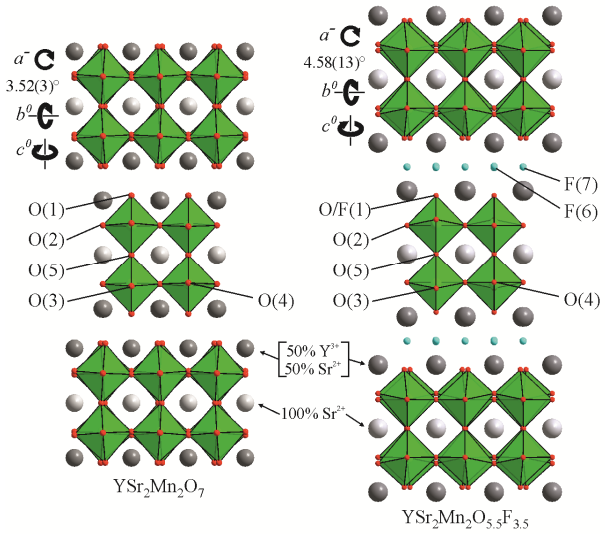

Figure 2. The structures of $YSr_2Mn_2O_7$ and $YSr_2Mn_2O_{5.5}F_{3.5}$.

$YSr_2Mn_2O_7$		$YSr_2Mn_2O_{5.5}F_{3.5}$		
Anion	BVS (O)	Anion	BVS (O)	BVS (F)
O(1)	1.711	X (1):O/F(1)	1.509	1.237
O(2)	2.225	X(2):O(1)	2.069	1.756
O(3)	2.227	X(3):O(3)	2.157	1.833
O(4)	2.236	X(4):O(4)	1.854	1.569
O(5)	1.974	X(5):O(5)	2.122	1.775
		X(6):F(6)	1.460	1.103
		X(7):F(7)	1.498	1.132

Table 3. Anion bond valence sums from $YSr_2Mn_2O_7$ and $YSr_2Mn_2O_{5.5}F_{3.5}$.

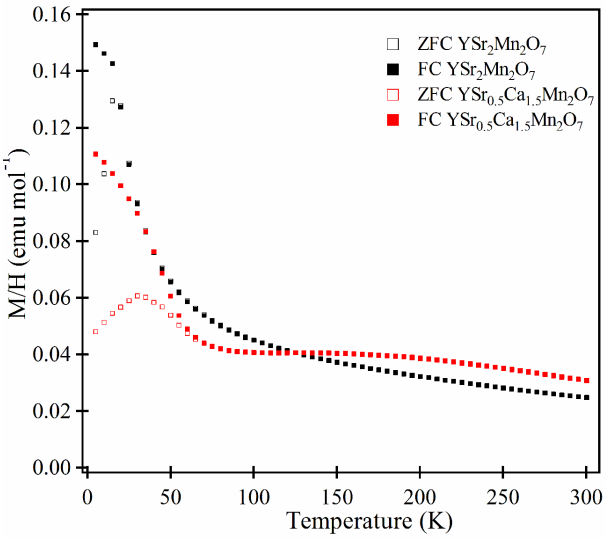

Figure 3. Zero-field cooled and field cooled magnetization data collected from $YSr_2Mn_2O_7$ and $YSr_{0.5}Ca_{1.5}Mn_2O_7$ in an applied filed of 100 Oe.

Magnetism. Zero-field cooled and field cooled magnetization data collected from $YSr_{0.5}Ca_{1.5}Mn_2O_7$ in an applied field of 100 Oe, shown in Figure 3, are qualitatively very similar to the analogous data collected from $YSr_2Mn_2O_7$, also shown in Figure 3. The later phase has been characterized as a spin-glass,[25] suggesting that $YSr_{0.5}Ca_{1.5}Mn_2O_7$ is also a spin-glass with a slightly elevated freezing temperature compared to $YSr_2Mn_2O_7$.

Discussion

Phase separation in $YSr_{2-x}Ca_xMn_2O_7$. The phase separation observed on calcium doping of $YSr_2Mn_2O_7$ is analogous to that reported for other $RESr_2Mn_2O_7$ (RE = Y, lanthanide) n = 2 Ruddlesden-Popper phases.[26-28] Previous studies focused on $RESr_2Mn_2O_7$ phases observed that it was generally only possible to prepare single phase samples for compositions containing small RE^{3+} cations (Tb-Er, Y) and that systems containing large RE^{3+} cations (La-Gd) split into two-phase mixtures.

This difference in behavior between the large and small A-cation systems has been attributed to the differing degrees of cation order these phases exhibit. Compositions containing small RE cations (Tb-Er, Y) order to place Sr^{2+} on the 12-coordinate A-sites, and a 1:1 mixture of Sr^{2+} and RE^{3+} on the 9-coordinate A-sites in the framework. As the size of RE^{3+} increases the degree of A-cation order diminishes and this is associated with samples separating into two or more different n = 2 Ruddlesden-Popper phases. The decline in the degree of A-cation order can be attributed to the reduction in the size difference between Sr^{2+} and RE^{3+} as the size of RE^{3+} increases.

The results of the calcium-for-strontium cation exchange of $YSr_2Mn_2O_7$ reported here support the association between the degree of A-cation order and single/multi-phase behavior. Low levels of calcium substitution (25-50%) lead to separation into two phases which appear to have similar compositions, but different degrees of A-cation order. In addition the two observed phases become more dissimilar as the concentration of calcium increases (Table 1). This behavior can be rationalized by observing that partial substitution of Sr^{2+} by Ca^{2+} makes the average size of the AE^{2+} (AE^{2+} = Ca^{2+}, Sr^{2+}) cations smaller, and therefore more similar to the size of Y^{3+}, disrupting the A-cation order of the host phase and leading to multiple-phase behavior. Thus the phase separation observed for $YSr_{2-x}Ca_xMn_2O_7$ ($0.25 < x < 1$) compositions can be seen as analogous to that observed for the $RESr_2Mn_2O_7$ phases as both are associated with the loss of A-cation order as the difference in the average radii of the RE^{3+} and AE^{2+} cations decreases.

Structural influence of calcium doping. It is surprising at first sight that replacing of 50% of the Sr^{2+} with Ca^{2+} leads to only a modest increase in the magnitude of the cooperative distortions of the $YSr_{2-x}Ca_xMn_2O_7$ framework, increasing the MnO_6 rotation angle from 3.52º at x = 0 to 7.12º in the majority phase at x = 1 (Figure 4) but leading to no change in structural symmetry. This despite the fact that the structural tolerance factor, calculated using ionic radii,[35] changes from t = 0.98 for $YSr_2Mn_2O_7$ to t = 0.95 for $YSrCaMn_2O_7$.

This modest structural response to cation substitution can be rationalized by observing that the majority of the substituted calcium cations reside on the 9-coordinate A-sites in the lattice. In contrast to the 12-coordinate A-cations sites, the A-O bond lengths of the 9-coordinate A-cation sites can be contracted, to accommodate a decline in average A-cation radius, by simply contracting the rock salt layers of the Ruddlesden-Popper framework along the z-axis. Such a contraction brings the perovskite blocks closer together without deforming the MnO_6 octahedra or requiring them to cooperatively rotate, leading to the observed contraction in c-lattice parameters on calcium substitution (Table 1), but only a modest change to the tilting distortion of the Mn-O framework. Thus, it is not until the cation substitution level exceeds 50%, and a significant concentration of Ca^{2+} resides on the 12-coordinate A-cation site, that a large increase in the magnitude of the MnO_6 tilts, and a change in lattice symmetry, is observed.

Crystal structure of $YSr_{0.5}Ca_{1.5}Mn_2O_7$. As shown in Figure 4, when 75% of the strontium is replaced by calcium the system changes symmetry to adopt an $a^-b^-c^-/b^-a^-c^-$ distorted lattice, in space group $P2_1/n11$. To the best of our knowledge this is the first report of an n = 2 Ruddlesden-Popper phase adopting this distortion pattern. Typically as the tolerance factor of a $P4_2/mnm$ $a^-b^0c^0/b^0a^-c^0$ distorted n = 2 Ruddlesden-Popper phases is reduced, the arrangement of titled octahedra changes to an $Amam$ $a^-a^-c^0/a^-a^-c^0$ distortion in which a rotation is added around the y-axis with the same magnitude as the x-axis, as observed during the cation substitution of $LnAE_2Fe_2O_7$ phases.[16] In contrast the lattice distortion observed for $YSr_{0.5}Ca_{1.5}Mn_2O_7$ maintains the large $a^-b^0c^0/b^0a^-c^0$ distortion component observed for $YSr_{2-x}Ca_xMn_2O_7$ x < 1 and adds small $a^0b^-c^0/b^-a^0c^0$ and $a^0b^0c^-/b^0a^0c^-$ components such that the average rotation angles are 8.74(12)º, 1.72(14)º and 0.89(25)º for a, b and c respectively. In terms of an irreducible

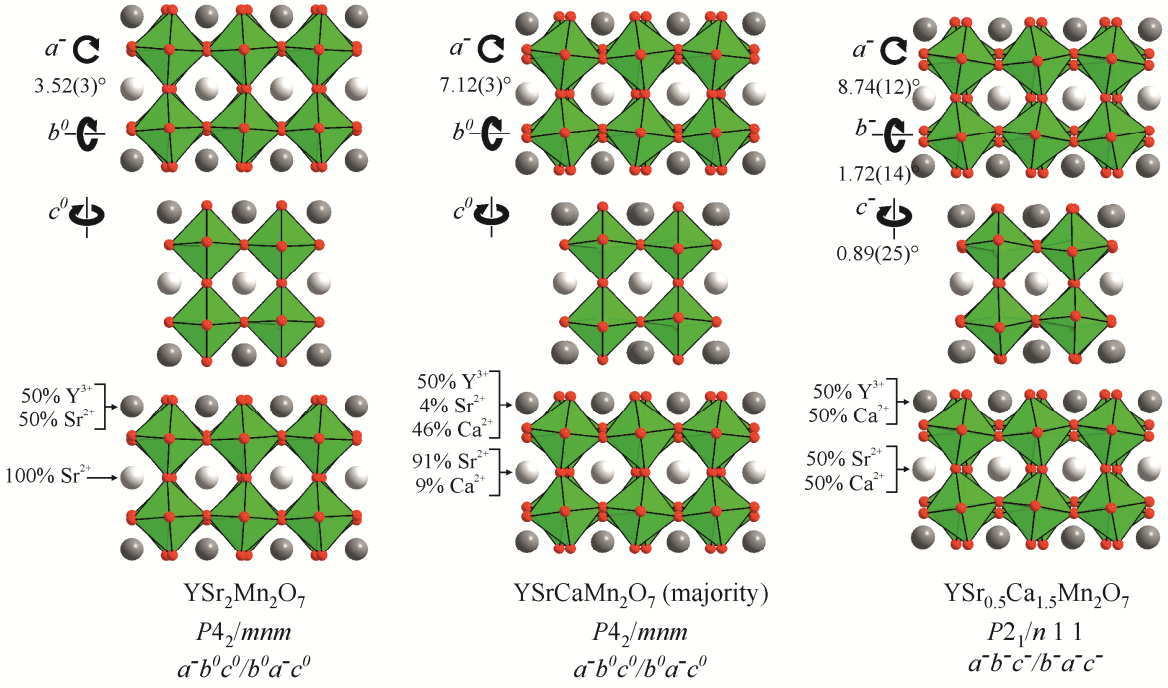

Figure 4. The structures of $YSr_{2-x}Ca_xMn_2O_7$ phases highlighting how the A-cation distribution and the collective tilting and twisting of the MnO_6 octahedra change with calcium content. Octahedral rotation angles were determined via O-O-O-O torsion angles as described in the Supporting Information.

representation (irrep) description, the octahedral tilting in the $P4_2/mnm$ $a^-b^0c^0/b^0a^-c^0$ structures (symmetry D_{4h}[14]) is described by a distortion mode which transforms as $X_3^-{}_{(a;a)}$. On lowering symmetry to $P2_1/n11$ (C_{2h}[5]) this $X_3^-{}_{(a;a)}$ mode becomes an $X_3^-{}_{(a;b)}$ mode leading to a change to an $a^-b^-c^0/b^-a^-c^0$ distortion which on the addition of an X_1^- distortion mode, becomes an $a^-b^-c^-/b^-a^-c^-$ distortion.

The reason for $YSr_{0.5}Ca_{1.5}Mn_2O_7$ adopting this unusual distortion pattern is not immediately clear. However, it should be noted that despite the extensive cation substitution the phase retains a high level of cation order such that the average radii of the cations on the 9- and 12-coordinate A-sites remains significantly different. It seems likely that this unusual feature is responsible for the novel octahedral tilting arrangement, although the microscopic mechanism by which it stabilizes this distortion is unclear.

Fluorination of $YSr_2Mn_2O_7$. In common with a number of other n = 2 Ruddlesden-Popper phases, topochemical fluorination of $YSr_2Mn_2O_7$ proceeds via a mixture of anion insertion and anion exchange to yield $YSr_2Mn_2O_{5.5}F_{3.5}$, in which fluoride ions have been inserted into tetrahedral coordination sites in the rock salt layers of the framework and also exchanged with 'apical' oxide ions in the perovskite sheets.

An unusual feature of this chemical transformation is that, unlike many analogous fluorination reactions, it is not accompanied by a change in crystallographic symmetry. Specifically fluorination of $YSr_2Mn_2O_7$ does not induce a cooperative twist of the $Mn(O/F)_6$ units around the *z*-axis – a structural deformation which is observed in a number of analogous fluorination reactions.[17-20]

The tendency for fluorination to induce a '*z*-twist' to the perovskite framework of n = 2 Ruddlesden-Popper oxide phases can be rationalized by observing that insertion of fluoride ions into the rock salt layers of the structure leads to a contraction of these blocks as the inserted fluoride ions pull the A-cations closer together. This contraction acts to constrict the *ab*-plane of the perovskite sheets, as indicated by a contraction of the *a* and *b* lattice parameters.[17-18, 20] In response the BO_6 octahedra cooperatively rotate around the *z*-axis to relive the bond strain induced by this *ab*-plane compression.

Comparing the structures of $YSr_2Mn_2O_7$ and $YSr_2Mn_2O_{5.5}F_{3.5}$ it can be seen that a similar contraction has occurred, with the area of the *ab*-plane declining from 29.20(1) Å^2 to 28.37(1) Å^2 on fluorination. However this contraction does not induce a *z*-twist into the perovskite framework because the concomitant oxidation of $Mn^{+3.5}$ to $Mn^{+3.75}$, which occurs on fluorination, leads to a contraction in the average Mn-O bond length, so the bond strain induced by the *ab*-plane contraction is much reduced and can be relieved by enhancing the *x*-twist of the parent oxide phase. This mechanism of strain relief is particularly effective for $YSr_2Mn_2O_{5.5}F_{3.5}$ because there is a large change in the <Mn-O> bond length on oxidation (6CN radii Mn^{3+} = 0.645 Å, Mn^{4+} = 0.530 Å)[35], compared to other elements, for example ruthenium (6CN radii Ru^{4+} = 0.620 Å, Ru^{5+} = 0.565 Å)[35] which is present in many of the other oxide-fluoride systems previously studied. Thus fluorination of $YSr_2Mn_2O_7$ to $YSr_2Mn_2O_{5.5}F_{3.5}$ leads to only a modest change in tilting distortion of the perovskite network, with the rotation of the MnX_6 units around the *x*-axis increasing from 3.52(3) ° to 4.58(13) °, without a change in crystallographic symmetry (Figure 2).

Conclusion

The cation ordered structure of $YSr_2Mn_2O_7$ incorporating an $a^-b^0c^0/b^0a^-c^0$ distortion is very robust to cation substitution and anion insertion. In order to modify the distortion mode of the structure by calcium-for-strontium exchange, 75% of the strontium must be exchanged to drive a change in crystallographic symmetry. Principally this is because the small Ca^{2+} cations are substituted preferentially on to the 9-coordinate A-site in the struc-

ture, which has only a small influence on the collective tilting distortions of the perovskite layers. Thus it could be argued that the A-cation order of the phase 'protects' the $a^-b^0c^0/b^0a^-c^0$ distorted lattice from modification by cation exchange, an further suggests that in general it will be hard to utilize cation doping of cation-ordered n = 2 Ruddlesden-Popper phases to induce non-centrosymmetric lattice distortions

$YSr_2Mn_2O_7$ also undergoes only minimal structural deformation on fluorine insertion due to the large contraction of the <Mn-O> bond lengths which compensate for the lattice contraction that occurs when fluoride ions are intercalated into the rock salt layers of the structure. These two effects mean that the Y-Sr-Ca-Mn-O-F system retains $a^-b^0c^0/b^0a^-c^0$ distorted perovskite blocks over a wide range of composition.

ASSOCIATED CONTENT

Supporting Information

Structural parameters, selected bond lengths and observed and calculated data from the structural refinements of $YSrCaMn_2O_7$, $YSr_{0.5}Ca_{1.5}Mn_2O_7$ and $YSr_2Mn_2O_{3.5}F_{5.5}$. A description of the method used for determining octahedral rotation angles from O-O-O-O torsion angles.

AUTHOR INFORMATION

Corresponding Author

*** Tel : +44 1865 272623. Fax: +44 1865 272690.**

email: michael.hayward@chem.ox.ac.uk

Author Contributions

All authors have given approval to the final version of the manuscript.

Notes

The authors declare no competing financial interests.

ACKNOWLEDGMENT

Experiments at the ISIS pulsed neutron facility were supported by a beam time allocation from the Science and Technology Facilities Council. WZ and PSH thank the Welch Foundation (Grant E-1457) and the NSF (DMR-1503573).

REFERENCES

1. Goldschmidt, V. M., *Naturwissenschaften* **1926,** *14*, 477.
2. Goodenough, J. B., *Localized to Itinerant Electronic Transition in Perovskite Oxides*. Springer-Verlag: Berlin, 2001.
3. Tilley, R. J. D., *Perovskites: Structure-Property Relationships*. John Wiley and Sons: Chichester 2016.
4. Benedek, N. A.; Rondinelli, J. M.; Djani, H.; Ghosez, P.; Lightfoot, P., Understanding Ferroelectricity in Layered Perovskites: New Ideas and Insights From Theory and Experiments. *Dalton Trans.* **2015,** *44*, 10543-10558.
5. Rondinelli, J. M.; Fennie, C. J., Octahedral Rotation-Induced Ferroelectricity in Cation Ordered Perovskites. *Adv. Mater.* **2012,** *24*, 1961-1968.
6. Knapp, M. C.; Woodward, P. M., A-site Cation Ordering in AA'BB'O_6 Perovskites. *J. Solid State Chem.* **2006,** *179*, 1076-1085.
7. King, G.; Woodward, P. M., Cation Ordering in Perovskites. *J. Mater. Chem.* **2010,** *20*, 5785-5796.
8. Bousquet, E.; Dawber, M.; Stucki, N.; Lichtensteiger, C.; Hermet, P.; Gariglio, S.; Triscone, J. M.; Ghosez, P., Improper Ferroelectricity in Perovskite Oxide Artificial Superlattices. *Nature* **2008,** *452*, 732-U4.
9. Benedek, N. A.; Fennie, C. J., Hybrid Improper Ferroelectricity: A Mechanism for Controllable Polarization-Magnetization Coupling. *Phys. Rev. Lett.* **2011,** *106*, 107204.
10. Mulder, A. T.; Benedek, N. A.; Rondinelli, J. M.; Fennie, C. J., Turning ABO_3 Antiferroelectrics into Ferroelectrics: Design Rules for Practical Rotation-Driven Ferroelectricity in Double Perovskites and $A_3B_2O_7$ Ruddlesden-Popper Compounds. *Advanced Functional Materials* **2013,** *23*, 4810-4820.
11. Oh, Y. S.; Luo, X.; Huang, F. T.; Wang, Y. Z.; Cheong, S. W., Experimental demonstration of hybrid improper ferroelectricity and the presence of abundant charged walls in (Ca, Sr)$_3$Ti$_2$O$_7$ crystals. *Nat. Mater.* **2015,** *14*, 407-413.
12. Cohen, R. E., Origin of Ferroelectricity in Perovskite Oxides. *Nature* **1992,** *358*, 136-138.
13. Kang, S. K.; Tang, H.; Albright, T. A., Structures for d^0 ML_6 and ML_5 Complexes. *J. Am. Chem. Soc.* **1993,** *115*, 1971-1981.
14. Kunz, M.; Brown, I. D., Out-of-Center Distortions around Octahedrally Coordinated d^0 Transition-Metals. *J. Solid State Chem.* **1995,** *115*, 395-406.
15. Pearson, R. G., The 2nd-Order Jahn-Teller Effect. *Theochem-Journal of Molecular Structure* **1983,** *12*, 25-34.
16. Pitcher, M. J.; Mandal, P.; Dyer, M. S.; Alaria, J.; Borisov, P.; Niu, H.; Claridge, J. B.; Rosseinsky, M. J., Tilt Engineering of Spontaneous Polarization and Magnetization Above 300 K in a Bulk Layered Perovskite. *Science* **2015,** *347*, 420-424.
17. Li, R. K.; Greaves, C., Double-Layered Ruthenate $Sr_3Ru_2O_7F_2$ Formed by Fluorine Insertion into $Sr_3Ru_2O_7$. *Phys. Rev. B* **2000,** *62*, 3811-3815.
18. Denis Romero, F.; Bingham, P. A.; Forder, S. D.; Hayward, M. A., Topochemical Flulorination of $Sr_3(M_{0.5}Ru_{0.5})_2O_7$ (M = Ti, Mn, Fe) n = 2 Ruddlesden-Popper Phases. *Inorg. Chem.* **2013,** *52*, 3388-3398.
19. Zhang, R.; Senn, M. S.; Hayward, M. A., Directed Lifting of Inversion Symmetry in Ruddlesden-Popper Oxide-Fluorides: Toward Ferroelectric and Multiferroic Behavior. *Chem. Mater.* **2016,** *28*, 8399-8406.
20. Zhang, R.; Read, G.; Lang, F.; Lancaster, T.; Blundell, S. J.; Hayward, M. A., $La_2SrCr_2O_7F_2$ - A Ruddlesden-Popper Oxyfluoride Containing Octahedrally Coordinated Cr^{4+} Centers. *Inorg. Chem.* **2016,** *55*, 3169-3174.
21. Luo, K.; Tran, T. T.; Halasyamani, P. S.; Hayward, M. A., Synthesis and Selective Topochemical Fluorination of the Cation and Anion-Vacancy Ordered Phases Ba_2YCoO_5 and $Ba_3YCo_2O_{7.5}$. *Inorg. Chem.* **2013,** *52*, 13762-13769.
22. Larson, A. C.; Von Dreele, R. B. *General Structure Analysis System*, Los Alamos National Laboratory Report LAUR 86-748: 2000.
23. Kurtz, S. K.; Perry, T. T., A Powder Technique for the Evaluation of Nonlinear Optical Material. *J. Appl. Phys.* **1968,** *39*, 3798-3813.
24. Ok, K. M.; Chi, E. O.; Halasyamani, P. S., Bulk characterization methods for non-centrosymmetric materials: second-harmonic generation, piezoelectricity, pyroelectricity, and ferroelectricity. *Chem. Soc. Rev.* **2006,** *35*, 710-717.
25. Battle, P. D.; Millburn, J. E.; Rosseinsky, M. J.; Spring, L. E.; Vente, J. F., Neutron Diffraction study of the structural and electronic propoerties of $Sr_2HoMn_2O_7$ and $Sr_2YMn_2O_7$. *Chem. Mater.* **1997,** *9*, 3136-3143.
26. Battle, P. D.; Green, M. A.; Laskey, N. S.; Millburn, J. E.; Murphy, L.; Rosseinsky, M. J.; Sullivan, S. P.; Vente, J. F., Layered Ruddlesden-Popper manganese oxides:synthesis and cation ordering. *Chem. Mater.* **1997,** *9*, 552-559.
27. Battle, P. D.; Cox, D. E.; Green, M. A.; Millburn, J. E.; Spring, L. E.; Radaelli, P. G.; Rosseinsky, M. J.; Vente, J. F., Antiferromagnetism, ferromagnetism, and phase separation in the GMR system $Sr_{2-x}La_{1+x}Mn_2O_7$. *Chem. Mater.* **1997,** *9*, 1042-1049.
28. Battle, P. D.; Green, M. A.; Laskey, N. S.; Millburn, J. E.; Radaelli, P. G.; Rosseinsky, M. J.; Sullivan, S. P.; Vente, J. F., Crystal and

magnetic structures of the colossal magnetoresistance manganates $Sr_{2-x}Nd_{1+x}Mn_2O_7$ (x=0.0, 0.1). *Phys. Rev. B* **1996,** *54*, 15967-15977.

29. Sears, V. F., Neutron Scattering Lengths and Cross Sections. *Neutron News* **1992,** *3*, 26-37.

30. Aleksandrov, K. S.; Bartolome, J., Octahedral Tilt Phases in Perovskite-like Crystals with Slabs Containing an Even Number of Octahedral Layers. *J. Phys.:Condens. Matter* **1994,** *6*, 8219-8235.

31. Gurusinghe, N. N. M.; Fones, J. C.; Marco, J. F.; Berry, F. J.; Greaves, C., Fluorine Insertion into the Ruddlesden-Popper Phase $La_2BaFe_2O_7$: The Structure and Magnetic Properties of $La_2BaFe_2O_5F_4$. *Dalton Trans.* **2014,** *43*, 2038-2043.

32. Case, G. S.; Hector, A. L.; Levason, W.; Needs, R. L.; Thomas, M. F.; Weller, M. T., Syntheses, powder neutron diffraction structures and Mossbauer studies of some complex iron oxyfluorides: $Sr_3Fe_2O_6F_{0.87}$, Sr_2FeO_3F and $Ba_2InFeO_5F_{0.68}$. *J. Mater. Chem.* **1999,** *9*, 2821-2827.

33. Brown, I. D.; Altermatt, D., Bond-Valence Parameters Obtained from a Systematic Analysis of the Inorganic Crystal Structure Database. *Acta Crystallogr., Sect. B : Strucut. Sci.* **1985,** *B41*, 244-247.

34. Brese, N. E.; O'Keeffee, M., Bond-Valence Parameters for Solids. *Acta Crystallogr., Sect. B : Strucut. Sci.* **1991,** *B47*, 192-197.

35. Shannon, R. D., Revised effective ionic radii. *Acta Cryst.* **1976,** *A32*, 751-766.

SYNOPSIS TOC

The $a^-b^0c^0/b^0a^-c^0$ distorted framework of the n = 2 Ruddlesden-Popper phase $YSr_2Mn_2O_7$ resists changing symmetry on either 50% Ca-for-Sr substitution of fluorine insertion. Substituting 75% of the strontium for calcium finally leads to a symmetry change to a novel $a^-b^-c^-/b^-a^-c^-$ distortion arrangement space group $P2_1/n11$). The resilience of the $a^-b^0c^0/b^0a^-c^0$ framework of $YSr_2Mn_2O_7$ to resist symmetry changing deformations as its composition is changed is attributed to the A-site cation order of the lattice.